Hydrological Sciences Journal

ISSN: (Print) (Online) Journal homepage: https://www.tandfonline.com/loi/thsj20

Water and energy balance of canopy interception as evidence of splash droplet evaporation hypothesis

Shigeki Murakami

To cite this article: Shigeki Murakami (2021): Water and energy balance of canopy interception as evidence of splash droplet evaporation hypothesis, Hydrological Sciences Journal, DOI: 10.1080/02626667.2021.1924378

To link to this article: https://doi.org/10.1080/02626667.2021.1924378

Accepted author version posted online: 04 May 2021.

Publisher: Taylor & Francis & IAHS

Journal: *Hydrological Sciences Journal*

DOI: 10.1080/02626667.2021.1924378

Water and energy balance of canopy interception as evidence of splash droplet evaporation hypothesis

Shigeki Murakami

Kyushu Research Center, Forestry and Forest Products Research Institute, Kumamoto, Japan

Kyushu Research Center, Forestry and Forest Products Research Institute, 4-11-16 Kurokami, Chuo, Kumamoto, 860-0862, Japan
E-mail: smura@affrc.go.jp

Water and energy balance of canopy interception as evidence of splash droplet evaporation hypothesis

Canopy interception I can be divided into three processes: evaporation during rainfall I_R, during storm break time I_{Sbt}, and after cessation of rainfall. Those values were measured using plastic Christmas tree stands, and it was found that I_R was much larger than I_{Sbt}. Though it is commonly accepted that wet canopy evaporation is major process of I, if so, I_{Sbt} must be greater than I_R because of higher potential evaporation during storm break time. It was also demonstrated that measured I_R was greater than calculated I_R using the Penman–Monteith (PM) equation that assumes wet surface evaporation. Splash droplet evaporation (SDE), described as splash droplets generated by a raindrop hitting the canopy evaporate, was alternative mechanism of I. SDE can elucidate $I_{Sbt} << I_R$; for larger rainfall amount, the number of splash droplets becomes higher. Calculated I_R was smaller than measured because the PM equation does not include SDE.

Keywords: Penman–Monteith equation; wet canopy evaporation; splash droplet evaporation

1. Introduction

Forest is the land surface with the greatest evapotranspiration on earth, because of large values of canopy interception I that amount to 11% to 48% of rainfall (Hörmann *et al*. 1996). I is dependent not only on rainfall amount but also on types of rainfall and tree structures. Hall (2003) simulated the effect of rainfall intensity which affects raindrop size on I using stochastic model. It was concluded that I is insensitive to the types of rainfall, contrary to some studies that showed rise in I with rainfall intensity mentioned later in this section. Hall (2003) also revealed that predicted I was not necessarily greater for trees with larger leaf area index, because leaves with waxy needles have small storage capacity. In Hall's paper the evaporation component was calculated using Rutter model (Rutter *et al*. 1971) which is a physically based method to estimate I considering micrometeorological factors, e.g. air temperature, relative humidity, wind

speed and radiation. Rutter *et al*. is based on the Penman–Monteith (PM) equation (Monteith 1965) that has been believed to be able to successfully reproduce measured values. Gash (1979) also used the equation in a different mathematical approach from that of Rutter *et al*. to estimate *I*, confirming the reproducibility. Both models, i.e. Rutter *et al*. and Gash, are based on the accuracy of the PM equation that calculates evaporation rate from wet canopy surface.

However, there are many papers that claim that the PM equation or equivalent heat balance equation underestimated *I* in comparison with *I* measured by the water budget method, and some of those works indicated that the underestimation is greater than one order of magnitude (Schellekens *et al*. 1999, van der Tol *et al*. 2003, Murakami 2007, Wallace and McJannet 2008, Ghimire *et al*. 2012, Hashino *et al*. 2010, Saito *et al*. 2013, Ghimire *et al*. 2017). The discrepancy between the PM equation based models and the measured data often occurred at the time of heavy rainfall.

Though Gash model (Gash 1979) along with the revised one (Gash *et al*. 1995) used the PM equation to calculate evaporation rate from the wet canopy surface, both Gash models can calculate the evaporation rate without applying the equation. That is to say, the evaporation rate is obtained analytically using gross precipitation P_G, throughfall and stemflow. Applying this method, many studies calculated evaporation rate from the wet canopy surface. The maximum values were typically around 0.5 mm/h to 1 mm/h (Schellekens *et al*. 1999, Carlyle-Moses and Price 1999, Park *et al*. 2000, Price and Carlyle-Moses 2003, Deguchi *et al*. 2006, Wallace and McJannet 2008). Evaporation of 1 mm/h requires latent heat of vaporization of 694 W/m^2, which is 51% of the solar constant. Such a large amount of energy and evaporation is impossible to reproduce by the models using measured meteorological data.

Another aspect of contradiction on *I* is that *I* is proportional to rainfall amount,

while the PM equation, i.e. calculation of wet surface evaporation, does not include any parameter on rainfall amount. The fact implies the PM equation cannot predict *I*. In case of the model in Hall (2003), rainfall intensity was included to calculate water storage on canopy. A possible alternative mechanism of *I* is splash droplet evaporation (SDE, Dunin *et al*. 1988, Murakami 2006, Dunkerley 2009). Micro droplets produced by a raindrop impacting on canopy surface evaporate in a moment even under high relative humidity RH due to a combined huge surface area. SDE cannot be calculated by the PM equation, since SDE is not evaporation from the wet surface and not considered in the equation. SDE can explain the proportional relationship between the amount of *I* and P_G expressed in mm, because the larger the rainfall amount is the more the number of droplets generated becomes.

In recent years increasing number of researches showed the data that support the validity of SDE hypothesis (Zabret and Šraj 2019, Zhang *et al*. 2019, Jeong *et al*. 2019, Liu and Zhao 2020, Jiménez-Rodríguez *et al*. 2021) and required detailed process of SDE (Allen *et al*. 2017, Fan *et al*. 2019, Levia *et al*. 2019). Nonetheless, SDE has not yet been proved directly and the details are unknown. Murakami and Toba (2013) used water balance approach with a measurement of single tree weight that enabled obtaining *I* with high temporal resolution. They measured *I* in artificial Christmas tree stands that made it easy to measure the single tree weight and that enabled to separate *I* into three components, during rainfall I_R, during the storm break time I_{Sbt}, and after the cessation of rainfall I_{Aft}. They showed that the major part of *I* was I_R, with I_{Sbt} almost zero and I_{Aft} contributing a small percentage, which suggests SDE is the major process of *I*. As a general trend, potential evaporation during rainfall is smaller than during storm break time because of lower RH, higher solar radiation and air temperature at the time of

storm break time. If wet surface evaporation would have been the main mechanism of I, I_R had been smaller than I_{Sbt}, but in actuality, the result was opposite.

In the present study, a full analysis of the data collected by Murakami and Toba (2013) was made, which was a preliminary study, using the PM equation to confirm the validity of the equation and to evaluate the degree of contribution of SDE. Specifically, the objective of this paper is 1) to analyse I_R and I_{Sbt} with higher temporal resolution than Murakami and Toba (2013) to evaluate the diurnal change and the response to micrometeorology, namely, meteorological factors in the vicinity of the site, 2) to evaluate the amount of SDE, and 3) to discuss the validity and limitations of the PM equation, the physics of small droplet evaporation and the heat source of latent heat of vaporization from a SDE's point of view.

2. Material and methods

2.1 Site and trays with trees

The experiment was conducted at Tohkamachi Experimental Station of the Forestry and Forest Products Research Institute, Tohkamachi, Japan, 37°07'53"N 138°46'00"E. Artificial Christmas trees made of polyvinyl chloride (PVC) and iron lines were placed on three trays outside, exposed to natural weather conditions (Fig. 1). Canopy diameters, the degree of canopy closure, and plant area index are shown in Table 1, along with tree height and stand density for each tray. Trees of original height 65 cm (small) and 150 cm (large) were used. Both Tray 1 and Tray 2 had the outer dimension of a 180-cm square. They were made of plywood with a waterproof coating and set at an average height of 120 cm above ground level. Forty-one small trees were set on both trays, but on Tray 2 the tree height was extended to 110 cm using plastic rods of 1.2-cm

diameter. The catchment area of the two trays was reduced to a 122.4-cm square, smaller than the outer dimension. Because rainwater near the edge of the tray might escape and thus caused error (i.e., the "edge effect"), we avoided collecting rainwater from the outermost row of trees. Tray 3 was a lysimeter consisting of wood plates and a plastic sheet placed on the ground, with the catchment area of a 360-cm square. The same number of large trees as Trays 1 and 2 was used on Tray 3. Tree height on Tray 3 was extended to 240 cm by iron pipes of 2.8-cm outer diameter. Additional trees were placed along the outer edge of Tray 3 to avoid the edge effect. The arrangement of trees on trays was schematically shown in Murakami and Toba (2013). Each tray drained rainwater to a tipping bucket flow meter (see next section) and discharge from the tray was defined as net precipitation P_N that comprised both throughfall and stemflow. The measurement began on June 24, 2012. Murakami and Toba (2013) began to measure on May 24, 2012; however, we used data from June 24 because that was when measurement of single tree weight began. On August 23, in the middle of the start and the end of the experiment, the number of trees on Trays 2 and 3 was reduced to 25; i.e., those stands were thinned. However, Tray 1 remained unthinned because it was the control. The experiment ended on October 26, 2012.

2.2 Instrumentation

P_G was measured using three rain gauges. These were a storage-type gauge (home-made of copper alloy, 22.7 cm in diameter) and two tipping-bucket gauges, one with 0.5 mm per tip (B-071-02-00, Yokokawa Denshi Co., Ltd., Tokyo) and the other 0.1 mm per tip (CTKF-0.1, Climatec Inc., Tokyo). Though the 0.1-mm gauge could measure the amount of rainfall, it was used to determine the temporal distribution of rainfall, e.g., the start and end of a rain event, because this gauge tended to underestimate rainfall

amount relative to the 0.5-mm gauge. Rainfall measured by the 0.1-mm gauge was corrected using either the storage-type or the 0.5-mm gauge, and analysed at a 5-minute interval (Appendix A gives a detailed description of the method).

Three tipping-bucket type flow meters, two with 500-ml per tip (UIZ-TB500, Uizin Co., Ltd., Tokyo, for Tray 1; J-271-01-00, Yokogawa Co., Ltd., Tokyo, for Tray 2) and the other 2000-ml per tip (UIZ-TB2000, Uizin Co., Ltd., Tokyo, for Tray 3), were used with a measurement interval of 5 minutes. The resolution of P_N for Trays 1 and 2 was 0.333 mm, and that of Tray 3 was 0.154 mm. Weight of a single tree on Trays 1 and 3 was measured every minute using an electric balance (UX4200S, Shimadzu Corporation, Kyoto, Japan) and a digital push-pull gauge (RX-20, Aikoh Engineering Co., Ltd., Osaka, Japan), respectively, to monitor the influence of gusts on water storage. Actually, the data fluctuated due to wind and a 5-minute average was used to calculate water balance. Tree weight on Tray 2 was assumed to be the same as that on Tray 1. Measurement resolution of tree weight was some 0.01 mm water equivalent on Trays 1 and 2, and around 0.1 mm on Tray 3, respectively, considering the influence of wind. Net radiation R_n (Q*7, Radiation and Energy Balance Systems, Seattle, Washington, USA), air temperature T_a with RH (Sato Keiryoki Mfg. Co., Ltd., Tokyo, No. 7435-00 Hygro-station SK-5RAD-SP), and wind speed u (Ikeda Keiki Co., Ltd., Tokyo, WM-30P) were measured above Tray 2. R_n, T_a with RH, and u were measured at 2.7 m, 2.5 m and 4.0 m above ground, respectively. The type of instrument for T_a and RH was an aspirated psychrometer with a platinum resistance thermometer for the dry and wet bulb sensors. The accuracy of T_a and RH was ±0.1 °C and ±1%, respectively. The interval of measurement for R_n, T_a, RH and u was 1 minute, but 5-minute average data were used for analysis.

2.3 Separation of rainfall into rain and sub-rain events

Rainfall is intermittent, and a rain event was defined if rainfall stopped for a certain period of time or more. The time duration to separate rainfall into each independent rain event was defined as separation time Spt, which was set at 6 hours. In other words, if it stopped raining for 6 hours or longer rainfall was divided into two independent rain events. During the rain event there may be a time when rainfall ceases temporarily, which was defined as the storm break time(s) Sbt (s). The rain event was divided into two or more sub-rain events with Sbt. In the present study Sbt was set at 20 minutes. The time of the start and the end of *i*-th sub-rain event (*i*-th storm break) was defined as t_{Rsi} and t_{Rei} (t_{Bsi} and t_{Bei}), respectively. Spt and Sbt satisfy the relationship 20 minutes ≤ Sbt < 6 hours ≤ Spt. There appear many acronyms, abbreviations and symbols hereafter, and they are listed in Table B1 in Appendix B.

A shorter Sbt is better in terms of temporal resolution. However, a too-short Sbt causes large error, because it takes some time for rainwater in the tray to reach the flow meter. Just after the end of a sub-rain event with high rainfall intensity, changes in drainage were too rapid and too large to measure correctly within such a short Sbt. A 20-minute Sbt was found to be optimal by trial and error.

2.4 Water balance on a rain event and a sub-rain event bases

On a rain-event basis, P_G, P_N and I have a simple relationship:

$$I = P_G - P_N \qquad (1)$$

When a rain event consists of n sub-rain events, i.e. n-1 storm break time, with total amount of P_G, it is expressed as

$$P_G = \sum_{i=1}^{n} P_{Gi} = \sum_{i=1}^{n} \int_{t_{Rsi}}^{t_{Rei}} R dt$$

$$= \sum_{i=1}^{n} \left[\int_{t_{Rsi}}^{t_{Rei}} D dt + \int_{t_{Rsi}}^{t_{Rei}} E dt \right] + \sum_{i=1}^{n-1} \left[\int_{t_{Bsi}}^{t_{Bei}} D dt + \int_{t_{Bsi}}^{t_{Bei}} E dt \right] + \Delta S$$

(2)

where P_{Gi} is P_G for the i-th sub-rain event, R is rainfall rate, D is drainage rate from the tray, E is evaporation rate. ΔS is the difference in water storage S between t_{Ren} and t_{Rs1}. It was assumed that S became zero at the end of Spt (= t_{Ren} + 6 hours), which meant that the canopy dried out before the next rain event. Under the assumption ΔS is zero in Eq. (2) S does not appear in Eq. (1).

I during a sub-rain event I_R is given by

$$I_R = \sum_{i=1}^{n} I_{Ri} = \sum_{i=1}^{n} \int_{t_{Rsi}}^{t_{Rei}} E dt = \sum_{i=1}^{n} \left[\int_{t_{Rsi}}^{t_{Rei}} R dt - \int_{t_{Rsi}}^{t_{Rei}} D dt - \Delta S_{Ri} \right]$$

(3)

where I_{Ri} is I_R for the i-th sub-rain event and ΔS_{Ri} is the difference in S between t_{Rei} and t_{Rsi}. Considering that $R = 0$ during Sbt, Eq. (2) gives I during Sbt (I_{Sbt}).

$$I_{Sbt} = 0 \qquad for\ n = 1$$

(4)

$$I_{Sbt} = \sum_{i=1}^{n-1} I_{Sbti} = \sum_{i=1}^{n-1} \int_{t_{Bsi}}^{t_{Bei}} E dt = \sum_{i=1}^{n-1} \left[- \int_{t_{Bsi}}^{t_{Bei}} D dt - \Delta S_{Bi} \right] \quad for\ n \geq 2$$

(5)

where I_{Sbti} is I_{Sbt} for the i-th Sbt, and ΔS_{Bi} (≤ 0) is the difference in S between t_{Bei} and t_{Bsi}.

ΔS in Eq. (2) is partitioned into drainage and evaporation after the cessation of rainfall. Hence, I after the cessation of rainfall is written as

$$I_{Aft} = \Delta S - \int_{t_{Ren}}^{t_{Ren+6}} D dt \tag{6}$$

On a rain event basis, I is calculated using P_G and P_N (Eq. (1)), but Eqs. (3)–(6) can also yield canopy interception, which is defined as I'.

$$I' = I_R + I_{Sbt} + I_{Aft} \tag{7}$$

Theoretically, Eqs. (1) and (7) yield the same result. However, they are not necessarily the same, because Eq. (1) is the difference between P_G and P_N, whereas Eq. (7) is calculated using P_G, P_N and S. S includes some errors that is independent of P_G and P_N, which can make a difference between I and I'.

Murakami and Toba (2013) analysed rain events with $P_G \geq 0.1$ mm. In the present study, rain events with $P_G \geq 0.5$ mm were considered because $P_N = 0$ for $P_G < 0.5$ mm. If data were missing at one tray or more, data for the period were not analysed, though Murakami and Toba used such data.

2.5 Wet canopy evaporation model using the PM equation for I_R and I_{Sbt}

Wet canopy evaporation model using the PM equation was applied that has the same structure as that of Saito *et al*. (2013), except for water storage calculation. In the present study, S was directly measured. However, Saito *et al*. estimated S using water

storage capacity and rainfall intensity. *I* was calculated for each sub-rain event and Sbt. I_{Afi} was not estimated using the model, but obtained using Eq. (6).

$$I_{R\_PM} = \sum_{i=1}^{n} I_{R\_PMi} = \sum_{i=1}^{n} \left[\int_{t_{Rsi}}^{t_{Rei}} E_{Cal} dt \right] \tag{8}$$

$$I_{Sbt\_PM} = 0 \qquad for\ n = 1 \tag{9}$$

$$I_{Sbt\_PM} = \sum_{i=1}^{n-1} I_{Sbt\_PMi} = \sum_{i=1}^{n-1} \left[\int_{t_{Bsi}}^{t_{Bei}} E_{Cal} dt \right] \qquad for\ n \geq 2 \tag{10}$$

$$E_{Cal} = E_{PM} \qquad for\ S > E_{PM} \cdot \Delta t \tag{11}$$

$$E_{Cal} = S/\Delta t \qquad for\ S \leq E_{PM} \cdot \Delta t \tag{12}$$

The subscript "PM" represents calculation using the PM equation, and *"i"* does the *i*-th sub-rain event or Sbt. The calculation was done at a 5-minute interval (Δt = 5 min), corresponding to the measurement interval of P_G and P_N. E_{PM} is the evaporation rate for a wet canopy surface, estimated by the PM equation:

$$E_{PM} = \frac{\Delta}{\lambda(\Delta + \gamma)} (R_n - G) + \frac{\rho C_P (q_S(T_a) - q(T_a))}{\lambda(\Delta + \gamma) r_a} \tag{13}$$

where Δ is slope of the saturated specific humidity versus temperature curve, R_n is net radiation, G is ground heat flux (assumed to be zero), ρ is air density, C_P is the specific heat of air, $q_S(T_a)$ and $q(T_a)$ are saturated specific humidity and specific humidity at air temperature T_a, respectively, λ is latent heat of vaporization, γ (= C_P/λ) is the psychrometric constant, and r_a is aerodynamic resistance.

$$r_a = \frac{1}{k^2 u}\left\{ln\left(\frac{z-d}{z_0}\right)\right\}^2 \quad (14)$$

where k is the von Karman constant (0.4). z is the reference height (4.0 m above the ground, where the anemometer was placed), d is zero plane distance, and z_0 is roughness height length. d and z_0 were assumed to be 0.78 times and 0.08 times the tree height, respectively (Hattori 1985).

2.6 Estimation of SDE

Canopy interception during rainfall I_R comprises wet surface evaporation and SDE. I_R is derived from water balance using Eq. (3), while wet surface evaporation during rainfall is calculated using Eq. (8) as I_{R_PM}. Therefore, SDE can be estimated as the difference between I_R and I_{R_PM}. Namely, Eq. (15) calculates a component of canopy interception caused by SDE, I_{SDE}.

$$I_{SDE} = I_R - I_{R\_PM} \quad (15)$$

3. Results

3.1 P_G and P_N for each Tray

All P_G and P_N analysed are shown in Table 2 on a rain event basis. Monthly total

rainfall and average air temperature at the site were, respectively, 191.5 mm and 24.6°C in July, 49.0 mm and 26.5°C in August, 215.5 mm and 23.0°C in September and 131.5 mm and 14.8°C in October. As mentioned in the section 2.4 some rain events were not analysed and not included in Table 2.

3.2 I, I_R, I_{Sbt} and I_{Aft} on a rain event basis

All panels in Fig. 2 show a clear linear relationship between P_G and I_R, with large determination coefficients $r^2 \geq 0.795$. I_{jR} denotes I_R for Tray j (j = 1, 2, and 3), with the same convention for I_{Sbt} and I_{Aft}. Data shown in Fig. 2 are almost the same with those in Murakami and Toba (2013). However, the period of data used (cf. the section 2.1) and the size of the minimum rain event analysed (cf. the section 2.4) were slightly different.

I_{Sbt} in each tray was nearly zero and tended to have negative values, which were caused by measurement error. This error was caused by the drainage term in Eq. (5) due to time lag. The details are described in Appendix C.

For $P_G \geq$ about 5 mm, I_{Aft} reached a plateau around 1 mm, 1 mm and 2 mm before thinning for Trays 1, 2 and 3, respectively (Fig. 2a to c). After thinning, these values were around 1, 0.5 and 1 mm (Fig. 2d to f), corresponding to the reduction in tree density for Trays 2 and 3. However, Tray 1, the control, maintained the same value.

As shown in Table 3 the difference between I and I' between trays was 7.5% or less that was within the measurement error. I/P_G changed from 10.8% to 21.7% throughout the experiment, which was comparable with that in actual forests, though the experiments were conducted using plastic trees. I_R was the major constituent of I, i.e. I_R/I ranged from 67.3% to 93.8%, while I_{Aft} was minor. Considering the error of the flow meters (Section 2.2), I_{Sbt} was reasonably measured and was close to zero.

3.3 Comparison of I_R and I_{R_PM}, I_{Sbt} and I_{Sbt_PM} on a rain event basis with I_{SDE}

Observed values (I_R and I_{Sbt}) and calculated ones (I_{R_PM} and I_{Sbt_PM}) are shown in Fig. 3. Before the thinning period, most I_{R_PM} were nearly zero, though there were a few exceptions, i.e. some values of I_{R_PM} are around 2 mm (Fig. 3a–c). I_{Sbt_PM} fit to I_{Sbt}, i.e., close to zero, except for two rain events with P_G of 5.0 mm and 110.2 mm (named as "Rain Event 1" in the next section) that had I_{Sbt_PM} between 8.1 mm and 11.3 mm. The cause of the large I_{Sbt_PM} for those two rain events is unsuitable parameterization for the periods with larger positive R_n than the others as discussed in the section 3.5. Each tray had a similar trend of reproducibility for I_{R_PM} and I_{Sbt_PM}, implying that not forest parameters but meteorological conditions mainly determined the calculated results. After the thinning period, estimated values of I_{R_PM} were greatly improved, even though many still underestimated I_R (Table 3, Fig. 3d–f). The reason why the reproducibility of I_{R_PM} got better the after-thinning period is described in the section 4.2. Reproducibility of I_{Sbt_PM} was much worse than that of the before-thinning period, with large scatter. In the after-thinning period, each tray had the same trend of reproducibility. The cause of poorer estimation of I_{Sbt_PM}, i.e., overestimation, after thinning was also attributed to large R_n with inappropriate parameterization discussed in the section 3.5.

In the before-thinning period I_{SDE} for each Tray was predominant process of I as I_{SDE}/I ranged from 52.0 to 58.3% (Table 3). In the after-thinning period I_{SDE}/I showed smaller values 26.0% in Trays 1 and 15.9% in Tray 3 (the cause is discussed in the sections 4.2 and 4.6). I_{SDE} was major process only in Tray 2 with I/I_{SDE} of 60.9% in the after-thinning period.

3.4 P_G, I_R, I_{R_PM} and I_{SDE} for four heavy rain events

As a general trend, the longer the rainfall duration is the more the number of sub-rain events becomes. Kondo *et al*. (1992) and Návar (2020) found that the rainfall duration tends to become longer with increasing rainfall amount, though the correlation between the two variables were not very high. As a consequence, the number of sub-rain events is expected to increase with the rainfall amount. A rain event with many sub-rain events tends to include larger variation in meteorological conditions than with less sub-rain events. Analysing such a rain event is an effective approach to investigate the response of canopy interception on meteorological factors. The two heaviest rain events were selected in the before-thinning and after-thinning periods, respectively (Table 2), and conducted a detailed analysis of P_G, I_R, I_{R_PM} and I_{SDE}. The before-thinning period had rain events with P_G of 110.2 mm (Rain Event 1 with 22 sub-rain events) and 31.0 mm (Rain Event 2 with 6 sub-rain events) as shown in Table 4. The two rain events accounted for 69.1% of total rainfall in the before-thinning period (Table 3). In the after-thinning period, we selected one with P_G of 36.4 mm (Rain Event 3 with 14 sub-rain events) and another with 84.9 mm (Rain Event 4 with 8 sub-rain events). The two rain events occupied 41.6% of total rainfall in the after-thinning period (Table 3). In Table 4 values of I/I' are 90.9% to 108.1%, which were within the range of measurement error, except for an outlier of 81.0% in Tray 3 for Rain Event 1 that might be concerned with the clogging up of the drain. Some of values of I_R/I and I_{SDE}/I were over 100% due to measurement errors. I_R was major component of I. I_{SDE} was also predominant process of I, though in Tray 3 I_{SDE}/I for Rain Events 3 and 4 were 13.3% and 33.5%, respectively, which were much smaller than the others (Table 4). It is estimated that wet surface evaporation was the major evaporation process in Tray 3 for Rain Events 3 and 4. During Rain Event 2 the values of I_{SDE}/I were larger than I_R/I in all

trays, while for all the other events that was not the case. I_{SDE} was calculated as the residual between I_R and I_{R_PM} as shown in Eq. (15). In all trays I_{R_PM} for Rain Event 2 were -0.2 (< 0) that meant water vapour condensed on trees in calculation. Negative values of I_{R_PM} seemingly boosted I_{SDE} whether actual SDE increased or not, which was the cause of $I_{SDE}/I > I_R/I$ during Rain Event 2.

Fig. 4a–d, corresponding to Rain Events 1–4, respectively, indicate the relationship between P_{Gi} and I_{jRi} where I_{jRi} is I_R for Tray j (i = 1, 2 and 3) for the i-th sub-rain event. Solid and open symbols represent I_{jRi} with $R_n \geq 0$ and $R_n < 0$, respectively. Regression lines shown in Fig. 4a–d were calculated irrespective of the sign of R_n. Eleven regression lines were calculated, all of which showed $r^2 \geq 0.5$ (range 0.574–0.999). In Tray 3 before thinning, the regression line for Rain Event 1 (Fig. 4a) was unavailable because of missing data. The largest I_{3Ri} in Fig. 4b for Tray 3 was 2.2 mm, but the value in Murakami and Toba (2013) was mistakenly presented as 4.1 mm. The inclination of the regression line for a certain tray was not necessarily constant in each period, i.e. the before-thinning or the after-thinning period. At the same time change in the inclination between rain events was different depending on the tray. For instance in Tray 2 the inclination between Rain Events 3 and 4 are almost the same (red broken lines in Fig. 4c and d), while in Tray 3 it drastically declines (black long dashed dotted lines in Fig. 4c and d). Fig. 4e–h, respectively, corresponding to Rain Events 1–4, show the relationship between I_{jR_PMi} and I_{jRi} for each tray. Regression lines were calculated for I_{jRi} with $R_n \geq 0$, and are shown if $r^2 \geq 0.5$. Four out of nine regression lines indicated $r^2 \geq 0.5$. All regression lines that were calculated combining I_{jRi} with both $R_n \geq 0$ and $R_n < 0$ resulted in $r^2 < 0.5$. Regression lines derived from I_{jRi} with $R_n < 0$ gave $r^2 < 0.5$. The results in Fig. 4 imply that I_{jR_PMi} can estimate I_{jRi} only when $R_n \geq 0$; however, the estimation using P_{Gi} on a sub-rain event basis (Fig. 4a–d) is much better

than that of I_{jR_PMi} (Fig. 4e–h). All I_{jR_PMi} with $R_n < 0$ were negative, but only a small number of data for I_{jRi} with $R_n < 0$ were negative.

3.5 P_G, I_{Sbt} and I_{Sbt_PM} for four heavy rain events

Fig. 5a–d, respectively, corresponding to Rain Events 1–4, show measured and calculated I during Sbt on a storm break time basis in Tray j, i.e., I_{jSbti} and I_{jSbt_PMi}, respectively. Though measured I_{Sbt} on a rain event basis tended to show negative values, e.g. typically -1mm, due to measurement errors (Fig. 2), those of I_{Sbt} on a storm break time basis were much smaller because they were divided into each storm break time. Specifically, I_{jSbti} with $R_n < 0$ ranged from −0.402 to 0.343 mm that was comparable with the measurement resolution of P_N in Trays 1 and 2 (0.333mm). All I_{jSbt_PMi} with $R_n < 0$ had negative values, with a minimum of −0.219 mm. Data of I_{jSbti} with $R_n \geq 0$ were within −0.735 to 0.428 mm. Nevertheless, I_{jSbt_PMi} with $R_n \geq 0$ seriously overestimated I_{jSbti}, except for Rain Event 2 (Fig. 5b) that had only one I_{jSbti} with $R_n \geq 0$. This overestimation was attributed to inappropriate parameterization.

As stated in the section 3.2 and Table 3, I_{Sbt} was nearly zero on a rain event basis both in before and after thinning periods. Unsuitable parameterization for the periods with $R_n \geq 0$ was the cause of overestimation originated from capillary water in trees. The details are described in Appendix D.

3.6 Time course of I_R, I_{R_PM}, I_{Sbt} and I_{Sbt_PM}

A couple of time series for measured and/or calculated components, P_G, S, $\sum_{i=1}^{n} I_{jRi}$, $\sum_{i=1}^{n} I_{jR\_PMi}$, $\sum_{i=1}^{n-1} I_{jSbti}$, $\sum_{i=1}^{n-1} I_{jSbt\_PMi}$ (hereafter the last four are denoted as ΣI_{jRi}, ΣI_{jR_PMi}, ΣI_{jSbti} and ΣI_{jSbt_PMi} for simplicity) potential evaporation E_{PM} calculated by the

PM equation, and micrometeorological data R_n, RH, T_a and u are shown in Figs. 6 and 7, which correspond to Rain Events 1 and 4, respectively. "Nighttime" in Figures represents from sunset to sunrise. The time course of ΣI_{jRi} and ΣI_{jSbti} are shown stepwise because they were calculated on a sub-rain event basis and on a Sbt basis, respectively, based on water balance. That means it took some time for rainwater on the tray and in the tube to reach the flowmeter, and 5 minutes was too short in many cases. Note that I_{jRi} and I_{jSbti} are the difference between ΣI_{jRi} and ΣI_{jRi-1}, and ΣI_{jSbti} and $\Sigma I_{jSbti-1}$ for $i \geq 2$, respectively, and $\Sigma I_{jR1} = I_{jR1}$ and $\Sigma I_{jSbt1} = I_{jSbt1}$ for i =1. Other data including ΣI_{jR_PMi} and ΣI_{jSbt_PMi} are plotted every 5 minutes.

Rain Event 1 (Fig. 6) began at 13:45 on July 6, 2012 Japan Standard Time. Water storage in Trays 1 and 3 (S_1 and S_3, respectively) increased or decreased with rainfall. As mentioned in the section 2.2, S_2 in Tray 2 was assumed the same as in Tray 1. For Tray 3, ΣI_{3Ri}, ΣI_{3R_PMi}, ΣI_{3Sbti} and ΣI_{3Sbt_PMi} are shown through 17:15 on July 6, because the drain of the tray clogged (the caption in Fig. 2). In Trays 1 and 2, ΣI_{jRi} increased with P_G throughout Rain Event 1, except for three sub-rain events (total decreases were 0.24 and 0.21 mm for Trays 1 and 2, respectively, but difficult to read from Fig. 6c because of small changes), which was caused by measurement errors. At the end of Rain Event 1, ΣI_{1Ri} and ΣI_{2Ri}, i.e. I_{1R} and I_{2R}, respectively, were 8.8 and 9.2 mm, but ΣI_{1R_PMi} and ΣI_{2R_PMi}, i.e. I_{1R_PM} and I_{2R_PM}, respectively, were only 1.6 and 2.2 mm (Fig. 6c–d, Table 4). The underestimation of ΣI_{jR_PMi} was attributed to negative E_{PM}, reflecting $R_n < 0$ during nighttime (Fig. 6g). During nighttime on July 7 through on July 8 ΣI_{jR_PMi} decreased (again difficult to read in Fig. 6d) that meant condensation not evaporation occurred. Condensation was also occurred during nighttime on September 30 through on October 1 (Fig. 7d).

The greatest discrepancy between I_R and I_{R_PM} during nighttime is shown in Fig. 4h and Fig. 7 (for i=2, 17:55 on September 30 through 0:00 on October 1). For the sub-rain event with P_{G2} = 59.6 mm, I_{1R2}, I_{2R2} and I_{3R2} were 4.2, 11.6 and 1.7 mm (open square on the middle left, circle on the upper left and triangle on the lower left in Fig. 4h that correspond to Fig. 7c for i=2), respectively, while changes in I_{1R_PM}, I_{2R_PM} and I_{3R_PM} between i=2 and i=1 were −0.1, −0.2 and −0.2 mm (in Fig. 7d).The PM equation did not function at all as a predictive method.

Obviously, I_{jRi} was controlled by P_{Gi} instead of I_{jR_PMi} that is E_{PM}, as seen in Fig. 4 a–d. Meteorological factors RH, T_a and u (except for R_n during daytime) do not necessarily correlate with E_{PM} but with R_n (Figs. 6 and 7). I_{jR_PMi} was valid only when $R_n \geq 0$, but R_n was independent of P_{Gi}. P_{Gi} controlled I_{jRi} and ΣI_{jRi}, regardless of the sign of R_n.

ΣI_{jSbti} in Figs. 6e and 7e are nearly equal to zero corresponding to those in Fig. 5a and 5d, respectively. However, in Figs. 6f and 7f ΣI_{jSbt_PMi} rise on daytime when E_{PM} shows high value due to large R_n that caused overestimation in combine with capillary water in the trees as mentioned in the previous section.

4. Discussion

4.1 Increase in I after thinning

There are some studies that showed I declined after thinning (Teklehaimanot *et al*. 1991, Sun *et al*. 2015, Shinohara *et al*. 2015) or diminished with decreasing stand density (Komatsu *et al*. 2008), but no study demonstrated rise in I after thinning. Unexpectedly, I in Tray 2 increased after thinning (Table 3, Fig. 2b and e, Fig. 3b and e). The increase in I was observed on a rain event basis and was proportional to the

rainfall amount for each rain event. That held true on a sub-rain event basis as shown in Fig. 4a−d. The largest rain event after thinning was Rain Event 4 and the time course is shown in Fig. 7. The water storage on Tray 2 (red circles in Fig. 7b) was the smallest among the three trays. That meant Tray 2 was the least evaporative with the smallest wet surface area. The values of r_a for Tray 2 before and after thinning were assumed identical, because the two stands had the same tree heights (Eq. (14)). Considering the smallest water storage and the values of r_a for Tray 2 I_{R_PM} and I_{Sbt_PM} after thinning must decrease in terms of wet canopy evaporation. After all, there is no prospect that the increase in I can be elucidated by the PM equation, i.e., wet surface evaporation. It is presumed that thinning in Tray 2 promoted production of splash droplets and/or ventilation, though it still has to be supported by additional measurements, analysis and studies.

4.2 Validity and limitations of the PM equation

During nighttime, almost all I_{jR_PMi} for Rain Events 1–4 was negative, reflecting $R_n < 0$, meaning that water vapour condensed on the canopy surface instead of evaporation (Fig. 4e–h). In contrast, the measurement showed that I_{jRi} with $R_n < 0$ had positive values (Fig. 4e−h, Figs. 6 and 7) except for some sub-rain events in Fig. 6, which was caused by measurement error (the section 3.6). The discrepancy between I_{jR_PMi} and I_{jRi} was very large, and it was obvious that the PM equation did not work at night when $R_n < 0$ (the section 3.6). The aerodynamic term (second term on the right side of Eq. (13)) was small during the sub-rain event because of high RH, especially when the wind was weak. In that case, the radiation term (first term on the right side of Eq. (13)) controlled E_{PM}. At night, R_n was negative and as a consequence, E_{PM} during the sub-rain event

became negative during nighttime (Figs. 6 and 7). In daytime, the aerodynamic term remained small during the sub-rain event, but more often than not, R_n became positive, resulting in $E_{PM} \geq 0$. The observation indicated that I_{jSbti} was nearly zero and that I_{jRi} accounted for the major part of I, irrespective of the sign of R_n, i.e. regardless of daytime or nighttime (Tables 3 and 4, Figs. 6 and 7). I_{jR_PMi} with $R_n \geq 0$ could reproduce I_{jRi} (Figs. 4e–h), but estimation using P_G was better than the model (Figs. 4a–d). The reproducibility of I_{R_PM} got better the after-thinning period (the section 3.3 and Fig. 3), because there were more rain events with $R_n \geq 0$ during rainfall after thinning than before thinning.

Tsukamoto *et al*. (1988) conducted a water balance experiment using a single Japanese cedar tree placed in the stand. They measured P_G, P_N and tree weight under natural rainfall on an hourly basis, showing that I_R was proportional to P_G for a sub-rain event with I_{Sbt} nearly zero. They also indicated that I_{Sbt} and/or I_{Aft} were close to zero if solar radiation was nil, but the values increased with increasing radiation. Although we used artificial Christmas trees, the results were the same as those of Tsukamoto *et al*. (1988). Ours and the study of Tsukamoto *et al*. are consistent with the observational fact that I_R is independent of the radiative energy received by the canopy. Similarly, Pearce *et al*. (1980) found that hourly evaporation rates during daytime and nighttime were the same. Thus, we conclude that the PM-based model contradicts the measurements, though it can work when $R_n > 0$.

I_{SDE} is calculated using Eq. (15) as the difference between I_R and I_{R_PM}, which means I_{SDE} declines with increasing positive R_n as I_{R_PM} is boosted by R_n. However, if SDE actually reduces with R_n or not remains a problem to be solved because in the present study I_{SDE} was not measured directly but the residual between measured I_R and calculated I_{R_PM}.

4.3 Do splash droplets drift or evaporate?

Some studies assert that small droplets are transported somewhere by turbulence instead of being eliminated by evaporation (Hashino *et al*. 2010, Saito *et al*. 2013). The foundation of such studies was that terminal velocities of droplets with diameters 10, 20 and 50 μm are, respectively, 0.3, 1.2 and 7.6 cm/s. This means that the droplets are easily transported by weak wind and do not fall on the ground, because they are aerosols. Nonetheless, airborne droplets are captured by canopy again and observed as fog precipitation. This results in a contradiction, because the precipitation increases P_N and reduces I. For example, in tropical montane cloud forests fog precipitation accounts for between 2% and 45% of incident annual rainfall (Bruijnzeel *et al*. 2011). In Japan it is reported that cloud water deposition was more than 100% of annual rainfall (Kobayashi *et al*. 2001; Igawa *et al*. 2002). Apart from the transport of small droplets, first and foremost, it is impossible for such droplets to survive in the air without evaporation, even under high RH. They can survive stably only when the air is in saturation or supersaturation with respect to liquid water. Though E_{PM} is a function of some meteorological variables, evaporation of a small droplet is a function of T_a and RH in addition to the initial diameter (Holterman 2003). That means SDE must be calculated independent of the PM equation. The big difference between wet surface evaporation and SDE is that the surface evaporation rate saturates if the surface is completely wet but the SDE rate increases with increasing the number of droplets and decreasing the diameter of the droplets. It implies a slight change in the splash droplet size distribution, which is dictated by the raindrop size distribution and tree structures, can make a significant difference in the amount of SDE.

Life time of a small droplet under RH of 95% and 99% is shown in Fig. 8. It is strongly dependent on RH and the initial diameter. Fig. 8 was calculated based on

Holterman (2003) that was developed to evaluate spray drift on agricultural chemicals. Another approach to calculate evaporation of a small droplet is the theory of cloud physics. Murakami (2006) estimated life time of a small droplet using the cloud physical approach (Beard and Pruppacher 1971) that included much more complicated mathematical processes. For the droplet of 50 μm in diameter with RH of 95% the estimated life times in Fig. 8 and Murakami (2006) were, respectively, 58 s and 73 s at 10°C, 48 s and 61 s at 15°C, and 13 s and 47 s at 25°C. Unfortunately, the discrepancy between the two methods was 362% at 25°C. Assuming RH of 96% instead of 95%, life times in Fig. 8 got longer and almost the same with those of Murakami (2006): 72 s at 10°C, 60 s at 15°C and 45 s at 25°C. Considering the measurement accuracy of RH, i.e. ±1% at best, both estimations are within the measurement error range.

As shown in Fig. 8 and Murakami (2006) splash droplets do not drift and survive in the air but evaporate and disappear during rainfall. If the splash droplet size distribution along with the production rate are measured, it is possible to calculate SDE. Splash droplet size distribution may be measured using an aerosol spectrometer. It is challenging but required for the development of forest hydrology.

4.4 Heat source of latent heat of vaporization

Stewart (1977) showed that in a pine forest when the canopy was wet, flux of the latent heat of vaporization exceeded net radiation, and they presumed that sensible heat originated upwind and was advected to the forest. Pearce *et al*. (1980) also concluded that not net radiation but advected energy drives evaporation of a wet canopy. However, it seems unlikely that the latent heat continues to advect during a long-lasting rainfall event, and if the advection had been the energy source, the PM equation that takes in

situ meteorological factors into consideration could have successfully predicted *I*. There must be alternative mechanism and source.

Latent heat of vaporization for I_{2R2} in Fig. 7 (for i=2, 17:55 September 30 to 0:00 October 1) was 1294 W/m^2, as large as the solar constant (1370 W/m^2). Jiménez-Rodríguez *et al*. (2021) pointed out that during rainfall the temperature difference between the forest floor and the air in forest makes atmosphere unstable that causes vertical mixing. This mechanism transports water vapour upward. However, it is difficult for soil to exchange heat with the atmosphere due to nearly zero wind speed at the ground surface. Clouds where condensation occurs constantly is the only possible heat source. There are four possible mechanisms for transport of energy from the base of the cloud to the canopy, and at the same time it works as removal mechanism of water vapour above the canopy. First, the original air mass at the ground surface is squeezed upward by falling raindrops and the ambient air dragged downward by those drops (Dunin *et al*., 1988). Second, an updraft driven by the difference of molar weight between water and dry air transports the vapour together with energy, called "evaporative force" (Makarieva and Gorshkov, 2007). Decrease in air volume caused by the removal of water vapour near the ground is essentially compensated by the downdraft. Third, an updraft is caused by a reduction of air volume in cloud due to water vapour condensation (Makarieva *et al*., 2013). Like the second processes, the downdraft occurs automatically to compensate for the updraft. Fourth, evaporation of water itself boosts air pressure around the canopy and makes updraft because it is an abrupt expansion: phase change from liquid to gas. That is the opposite process of the third one and is proposed in the present study for the first time. The four processes have not received much attention and have not been widely accepted. None of them has been proved by measurements and they are still hypotheses, however, those processes can

elucidate the enigmatic problems: the removal mechanism of water vapour from the canopy during rainfall, the heat source (i.e., latent heat released in the cloud upon condensation of water vapour), and the supply of sensible heat from the cloud (Murakami 2006). Vertical mixing of air between the ground surface and the cloud base provides a simple answer for the heat source enigma. Because water vapour and energy are always balanced by rapid vertical mixing, variation in T_a and RH caused by the exchange between the cloud and the ground surface are seemingly not observed.

4.5. Rainfall intensity, types of rainfall and traits of vegetation

As mentioned in Introduction, simulation using the PM equation revealed that I was insensitive to rainfall intensity (Hall 2003). However, many studies including this present one showed that I increases with increasing rainfall amount or intensity, because actual evaporation process includes both wet surface evaporation and SDE, while Hall (2003) considered only wet surface evaporation.

Change in the inclination of the regression lines between rain events was different depending on the tray (Fig. 4a−d, the section 3.4). That would be caused by the difference in rainfall intensity. In the after-thinning period I_{SDE}/I was 26.0% in Tray 1 and 15.9% in Tray 3 (Table 3), but in the same period on a rain event basis it was 56.4% (Rain Event 3) and 69.5% (Rain event 4) in Tray 1 and 33.5% (Ran Event 4) in Tray 3 (Table 4). The difference in I_{SDE}/I on the period basis in Table 3 and on the rain event basis in Table 4 was more than double that would also be caused by the change in rainfall intensity. Larger I_{SDE}/I would be the result of higher rainfall intensity that can produce more splash droplets. Actually, I_{SDE}/I in Rian Event 4 (rainfall intensity derived from Table 2 was 3.7 mm/hour) was greater than that in Rain Event 3 (2.0 mm/hour) in all trays (Table 4).

The influence of rainfall intensity on rainwater partitioning including I is dependent on vegetation types. Janeau *et al*. (2015) showed that throughfall changes not only with rainfall intensity but also with vegetation types. In low rainfall intensity vegetation with flexible leaves had high interception ability and yielded much stemflow, but in high rainfall intensity it showed less interception ability due to flexibility of leaves falling rain water down. Contrary, vegetation with rigid leaves had high interception ability in both low and high rainfall intensities because of resistance against raindrop impact. In some vegetation shape of leaf is more important than leaf amount. Liu and Zhao (2020) pointed out that *Artemisia sacrorum Ledeb* (less leaf amount, canopy cover and leaf area but a fragmented leaf) showed less throughfall in comparison with *Spiraea pubescens Turcz* (larger leaf amount, canopy cover and leaf area but a compact leaf) probably due to effective splash droplets production.

Considering above-mentioned facts, the amount of I is dependent on both characteristics of trees and types of rainfall, e.g. drizzle, widespread rain and thunderstorm, because types of rainfall is relevant to raindrop size distribution (Seela *et al*. 2018). However, there are few studies focusing on the relationship between traits of trees, types of rainfall and I. To deal with the issue SDE is a key process that should be taken into account as SDE is dictated by those factors.

5. Conclusions

When net radiation R_n was positive, the PM equation could predict measured canopy interception during rainfall I_R, though the accuracy was not high enough. However, the equation could not do so during nighttime and when R_n was zero or negative. In many cases I_R was much larger than the predicted canopy interception using the PM equation I_{R_PM}, which proved wet canopy evaporation is the minor process and SDE dictates canopy interception. Specifically, the ratio of SDE to total canopy interception, I_{SDE}/I,

accounted for 52.0% to 58.3% and 15.9% to 60.9% in the before-thinning and the after-thinning periods, respectively, and on a rain event basis for nine out of eleven rain events I_{SDE}/I was over 56.4%.

The best predictor of I_R (and I also) was gross rainfall P_G. I_R and P_G had a proportional relationship that implied that rainfall itself is the driver of I_R. SDE could elucidate the proportional relationship between I_R and P_G, which is another evidence of SDE hypothesis. Calculation indicated that splash droplets do not drift and survive during rainfall but evaporate and disappear in a short time even under high relative humidity, e.g. 99%.

Considering the latent heat of vaporization required, clouds are the only possible heat source. Vertical mixing of air between the ground surface and the cloud base caused by the difference in molar weight of gases, falling raindrops, condensation in the clouds and evaporation of canopy interception can be the driving force. However, there is little theoretical and observational knowledge of the transport mechanism during rainfall, so this knowledge should be pursued.

I depends not only on P_G or rainfall intensity but also on rainfall types and tree characteristics, though the relationship between I and types of rainfall and/or tree properties is little known. Those unknown part of canopy interception processes are strongly associated with SDE.

Acknowledgements

I am grateful to two anonymous reviewers for useful and instructive comments. This study was financially supported by JSPS KAKENHI Grant Number 23580216.

Disclosure statement

The author has no conflicts of interest relevant to this article.

References

Allen, S.T., *et al*., 2017. The role of stable isotopes in understanding rainfall interception processes: a review. *WIREs Water*, 4:e1187, doi: 10.1002/wat2.1187

Beard, K.V. and Pruppacher, H.R., 1971. A wind tunnel investigation of the rate of evaporation of small water drops falling at terminal velocity in air. *Journal of Atmospheric Sciences*, 28, 1455–1464. doi: 10.1175/1520-0469(1971)028<1455:AWTIOT>2.0.CO;2

Bruijnzeel, L.A., Mulligan, M., Scatena, F.N., 2011. Hydrometeorology of tropical montane cloud forests: emerging patterns. *Hydrological Processes*, 25, 465–498. doi: 10.1002/hyp.7974

Carlyle-Moses D.E. and Price A.G., 1999. An evaluation of the Gash interception model in a northern hardwood stand. *Journal of Hydrology*, 214, 103–110. doi: 10.1016/S0022-1694(98)00274-1

Deguchi, A., Hattori, S. and Park, H., 2006. The influence of seasonal changes in canopy structure on interception loss: application of the revised Gash model. *Journal of Hydrology*, 319, 80–102. doi: 10.1016/j.jhydrol.2005.06.005

Dunin, F.X., O'Loughlin, E.M. and Reyenga, W., 1988. Interception loss from eucalypt forest: Lysimeter determination of hourly rates for long term evaluation. *Hydrological Processes*, 2 (4), 315–329. doi:10.1002/hyp.3360020403

Dunkerley, D.L., 2009. Evaporation of impact water droplets in interception processes: Historical precedence of the hypothesis and a brief literature overview. *Journal of Hydrology*, 376 (3–4), 599–604. doi: 10.1016/j.jhydrol.2009.08.004.

Fan, Y., *et al*., 2019. Reconciling Canopy Interception Parameterization and Rainfall Forcing Frequency in the Community Land Model for Simulating Evapotranspiration of Rainforests and Oil Palm Plantations in Indonesia. *Journal of Advances in Modeling Earth Systems*, 11(3), 732–751. doi: 10.1029/2018MS001490

Gash, J.H.C., 1979. An analytical model of rainfall interception by forests. *Quarterly Journal of the Royal Meteorological Society*, 105 (443), 43–55. doi:10.1002/qj.49710544304

Gash, J.H.C., Lloyd, C.R. and Lachaud, G., 1995. Estimating sparse forest rainfall interception with an analytical model. *Journal of Hydrology*, 170, 79–86. doi: 10.1016/0022-1694(95)02697-N

Ghimire,C.P., *et al*., 2012. Rainfall interception by natural and planted forests in the Middle Mountains of Central Nepal. *Journal of Hydrology*, 475, 270–280. doi:10.1016/j.jhydrol.2012.09.051

Ghimire,C.P., *et al*., 2017. Measurement and modeling of rainfall interception by two differently aged secondary forests in upland eastern Madagascar. *Journal of Hydrology*, 545, 212-225. doi:10.1016/j.jhydrol.2016.10.032

Hall, R.L. 2003. Interception loss as a function of rainfall and forest types: stochastic modelling for tropical canopies revisited. Journal of Hydrology, 280, 1-12. doi: 10.1016/S0022-1694(03)00076-3

Hashino, M., Yao, H. and Tamura, T., 2010. Micro-droplet flux in forest and its contribution to interception loss of rainfall – theoretical study and field experiment. *Journal of Water Resource and Protection*, 2 (10), 872–879. doi:10.4236/jwarp.2010.210104

Hattori, S., 1985. Explanation on derivation process of equations to estimate evapotranspiration and problems on the application to forest stand. *Bulletin of the Forestry and Forest Products Research Institute*, 332, 139–165 (in Japanese).

Holterman, H.J., 2003. Kinetics and evaporation of water drops in air. IMAG Report No. 2003-12, Wageningen, The Netherlands.

Hörmann, G., *et al*., 1996. Calculation and simulation of wind controlled canopy interception of a beechforest in northern Germany. *Agricultural and Forest Meteorology*, 79 (3), 131–148. doi:10.1016/0168-1923(95)02275-9

Igawa, M., Tsutsumi, Y. and Okochi, H., 2002. High frequency and large deposition of acid fog on high elevation. *Environmental Science and Technology*, 32: 1–6. doi: 10.1021/es0105358

Janeau, J.L., Grellier, S. and Podwojewski, P., 2015. Influence of rainfall interception by endemic plants versus short cycle crops on water infiltration in high altitude ecosystems of Ecuador. *Hydrology Research*, 46, 1008-1018. doi: 10.2166/nh.2015.203

Jeong, S., Otsuki, K. and Farahnak, M., 2019. Relationship between stand structures and rainfall partitioning in dense unmanaged Japanese cypress plantations. *Journal of Agricultural Meteorology*, 75, 92–102. doi: 10.2480/agrmet.D-18-00030.

Jiménez-Rodríguez, C. D., *et al*., 2021. Vapor plumes in a tropical wet forest: spotting the invisible evaporation. *Hydrology and Earth System Sciences*, 25, 619–635, doi: 10.5194/hess-25-619-2021, 2021

Kobayashi, T. *et al*., 2001. Cloud water deposition to forest canopies of *Cryptomeria japonica* at Mt. Rokko. *Water, Air, and Soil Pollution*, 130: 601–606. doi: 10.1023/A:1013859403320

Komatsu, H., *et al*., 2008. Relationship between annual rainfall and interception ratio for forests across Japan. *Forest Ecology and Management*, 256 (5), 1189–1197. doi:10.1016/j.foreco.2008.06.036

Kondo, J., *et al*., 1992. Shinrin niokeru kouuno shadan jyohastu no moderu keisan (A study on the modelling of rainfall interception in forests). *Tenki,* 39 (3), 159–168 (in Japanese). https://www.metsoc.jp/tenki/pdf/1992/1992_03_0159.pdf

Levia, 2019. D.F., *et al*., 2019. Throughfall partitioning by trees. *Hydrological Processes*, 33(12), 1698-1708. doi: 10.1002/hyp.13432

Liu, Y. and Zhao, L., 2020. Effect of Plant Morphological Traits on Throughfall, Soil Moisture, and Runoff. *Water*, 12, 1731, doi:10.3390/w12061731

Makarieva, A.M. and Gorshkov, V.G., 2007. Biotic pump of atmospheric moisture as driver of the hydrological cycle on land. *Hydrology and Earth System Sciences*, 11, 1013–1033. doi:10.5194/hess-11-1013-2007

Makarieva, A.M., *et al*., 2013. Where do winds come from? A new theory on how water vapor condensation influences atmospheric pressure and dynamics. *Atmospheric Chemistry and Physics*, 13, 1039–1056. doi:10.5194/acp-13-1039-2013

Monteith, J.L., 1965. Evaporation and the environment. *Symposium of the Society of Experimental Biology*, 19, 245–269.

Murakami, S., 2006. A proposal for a new forest canopy interception mechanism: Splash droplet evaporation. *Journal of Hydrology*, 319 (1–4), 72–82. doi:10.1016/j.jhydrol.2005.07.002

Murakami, S., 2007. Application of three canopy interception models to a young stand of Japanese cypress and interpretation in terms of interception mechanism. *Journal of Hydrology*, 342 (3–4), 305–319. doi:10.1016/j.jhydrol.2007.05.032

Murakami, S. and Toba, T., 2013. Experimental study on canopy interception using artificial Christmas trees to evaluate evaporation during rainfall and the effects of tree height and thinning. *Hydrological Research Letters*, 7, 91–96. doi: 10.3178/hrl.7.91

Návar, J., 2020. Modeling rainfall interception loss components of forests. *Journal of Hydrology*, 584, 124449. doi: 10.1016/j.jhydrol.2019.124449

Park, H.T., Hattori, S. and Kang, H.M., 2000. Seasonal and inter-plot variations of stemflow, throughfall and interception loss in two deciduous broad-leaved forests. *Journal of Japanese Society of Hydrology and Water Resources*, 13, 17–30. doi: 10.3178/jjshwr.13.17

Pearce, A.J., Rowe, L.K. and Stewart, J.B., 1980. Nighttime, wet canopy evaporation rates and the water balance of an evergreen mixed forest. *Water Resources Research*, 16 (5), 955–959. doi:10.1029/WR016i005p00955

Price A.G. and Carlyle-Moses D.E., 2003. Measurement and modelling of growing-season canopy water fluxes in a mature mixed deciduous forest stand, southern Ontario, Canada. *Agricultural Meteorology*, 119, 69–85. doi: 10.1016/S0168-1923(03)00117-5

Rutter, A., *et al*., 1971. A predictive model of rainfall interception in forest: I. Derivation of the model from observation in a plantation of Corsican pine. *Agricultural Meteorology*, 9, 367–384. doi:10.1016/0002-1571(71)90034-3

Saito, T., *et al*., 2013. Forest canopy interception loss exceeds wet canopy evaporation in Japanese cypress (Hinoki) and Japanese cedar (Sugi) plantations. *Journal of Hydrology*, 507, 287–299. doi:10.1016/j.jhydrol.2013.09.053

Schellekens, J., *et al*., 1999. Modelling rainfall interception by a lowland tropical rain forest in northern Puerto Rico. *Journal of Hydrology*, 225 (3–4), 168–184. doi:10.1016/S0022-1694(99)00157-2

Seela, B.K. *et al*., 2018. Raindrop Size Distribution Characteristics of Summer and Winter Season Rainfall Over North Taiwan. *Journal of Geophysical Research*, 123 (20), 11602-11624. doi: 10.1029/2018JD028307

Shinohara, Y., *et al*., 2015. Comparative modeling of the effects of intensive thinning on canopy interception loss in a Japanese cedar (Cryptomeria japonica D. Don) forest of western Japan. *Agricultural and Forest Meteorology*, 214-215, 148-156. doi:10.1016/j.agrformet.2015.08.257

Stewart, J.B., 1977. Evaporation from the wet canopy of a pine forest. *Water Resources Research*, 13, 915–921. doi:10.1029/WR013i006p00915

Sun, X., *et al*., 2015. Effect of strip thinning on rainfall interception in a Japanese cypress plantation. *Journal of Hydrology*, 252, 607–618. doi:10.1016/j.jhydrol.2015.04.023

Teklehaimanot, Z., Jarvis, P.G. and Ledger, D.C., 1991. Rainfall interception and boundary layer conductance in relation to tree spacing. *Journal of Hydrology*, 123 (3–4), 261–278. doi: 10.1016/0022-1694(91)90094-X

Tsukamoto, Y., Tange, I. and Minemura, T., 1988. Interception loss from forest canopies. *Hakyuchi-kenkyu* (*Bulletin of the Institute for Agricultural Research on Rolling Land*). 6, 60–82 (in Japanese with English summary).

van der Tol, C., *et al*., 2003. Average wet canopy evaporation for a Sitka spruce forest derived using the eddy correlation-energy balance technique. *Journal of Hydrology*, 276 (1–4), 12–19. doi:10.1016/S0022-1694(03)00024-6

Wallace, J. and McJannet D., 2008. Modelling interception in coastal and montane rainforests in northern Queensland, Australia. *Journal of Hydrology*, 348, 480–495. doi:10.1016/j.jhydrol.2007.10.019

Zabret, K. and Šraj, M., 2019. Evaluating the Influence of Rain Event Characteristics on Rainfall Interception by Urban Trees Using Multiple Correspondence Analysis. *Water*, 11, 2659; doi:10.3390/w11122659

Zhang, J., *et al*., 2019. Typhoon-induced changes in rainfall interception loss from a tropical multispecies 'reforest'. *Journal of Hydrology*, 568, 658–675. doi: 10.1016/j.jhydrol.2018.11.024

Appendix A

Modification of rainfall amount measured by the 0.1-mm rain gauge

The 0.1-mm rain gauge underestimated rainfall amount in comparison with that of the storage-type and the 0.5-mm gauge, but the degree of underestimation varied depending on the rain event. For example, for one rain event that started on July 6 the rainfall amount measured by the storage-type, the 0.5-mm and the 0.1-mm gauge was 110.2 mm, 110.5 mm and 104.3 mm (94.6% of the storage-type gauge), respectively, while for another rain event on September 6 the amount of rainfall measured by the storage-type, the 0.5-mm and the 0.1-mm gauge was 27.0 mm, 27.0 mm and 24.4 mm (90.4% of the storage-type gauge), respectively (cf. Table 2). Thus, either the storage-type or the 0.5-mm gauge was used to measure the rainfall amount. Rainfall of the storage gauge was measured manually at least every few days on weekdays but omitted on a day off. Rainfall amount measured by the 0.1-mm gauge was modified based on that of the storage-type gauge on a rain event basis, but was corrected based on data measured by the 0.5-mm gauge when storage gauge data were missing. P_G was analysed at a 5-minute interval.

Appendix C

Cause of negative values of I_{Sbt} in Fig. 2

Ideally, rainwater stored on the stand *S* at the end of a sub-rain event would have been the only drainage source during the subsequent *Sbt*. However, in actuality, at the end of the sub-rain event, rainwater that would have drained during that sub-rain event from the trees prior to the *Sbt* of interest remained on the tray and in the tube leading to the flow meters. The remaining rainwater was supplied as runoff *D* in Eq. (5), resulting in negative I_{Sbt}. The storage term in Eq. (5), ΔS_{Bi}, is always negative or zero, i.e., $-\Delta S_{Bi} \geq 0$. Normally, the error caused by ΔS_{Bi} is smaller than that of the drainage term, because *S* measured by weighing devices has no delay time like drainage from trays, as well as a resolution higher than that of the drainage measurement (the section 2.2.).

Appendix D

Cause of overestimation of I_{Sbt_PM}

According to Eqs. 8–12, evaporation rate $E_{Cal} = E_{PM}$ for $S > E\_{PM}\cdot\Delta t$; otherwise, $E_{cal} = S/\Delta t$. Assuming that E_{PM} is sufficiently large for a wet canopy surface to dry out during *Sbt* and $S = 0$ is reached, $E_{Cal} = S/\Delta t = 0$ at the end of *Sbt*. However, the trees did not always dry out ($S \neq 0$), even when E_{PM} maintained a large value over a long period. This was because under certain conditions, rainwater was not on the surface of the canopy but existed as capillary water. The trees were made of PVC imitation leaves that were inserted in twisted iron lines. Rainwater was stored in the spaces of the twisted iron lines and PVC leaves as capillary water, which was difficult to evaporate. In other words, the actual r_a was much larger than that calculated by Eq. (14). Because the objective of the present study was not to reproduce I_{Sbt} but to evaluate the amount of SDE and the validity and limitations of the PM equation, optimization of r_a for I_{jSbt_PMi} with $R_n \geq 0$ was not carried out.

Table 1 Stand structure of each tray before and after thinning.

	Tray number		1	2	3
	Tree height	(cm)	65	110	240
	Tree height from the ground	(cm)	185	230	240
	Canopy diameter	(cm)	30	30	75
Jun. 24 to Aug. 23, 2012					
Before thinning	Number of trees	(trees/tray)	41	41	41
	Plant area index*	(m^2/m^2)	5.1	5.1	5.9
	Canopy closure	(%)	96	96	94
	Water storage capacity S_{max}**	(mm)	2.0	2.0	3.8
Aug. 24 to Oct. 26, 2012					
After thinning	Number of trees	(trees/tray)	41	25	25
	Plant area index*	(m^2/m^2)	5.1	1.8	2.9
	Canopy closure	(%)	96	58	79
	Water storage capacity S_{max}**	(mm)	2.0	1.2	2.3

* Measured by LAI-2000 (LI-COR, NE, USA)

** Measured by weighing a tree one minute after pouring water over the tree

Table 2 Gross rainfall P_G and net rainfall P_N for each tray on a rain event basis.

Start of rain event		Duration	P_G	P_N Tray 1	P_N Tray 2	P_N Tray 3	Rain Event number
		(hours)	(mm)	(mm)	(mm)	(mm)	
2012/7/1	16:00	10.3	4.5	3.3	3.0	2.6	
2012/7/2	8:35	0.2	0.5	0.3	0.0	0.2	
2012/7/6	13:45	52.2	110.2	101.3	101.6	98.5	Rain Event 1
2012/7/12	0:15	16.7	5.0	3.0	2.0	2.3	
2012/7/13	2:45	0.3	0.5	0.3	0.3	0.0	
2012/7/14	0:30	8.6	13.0	12.3	12.0	11.4	
2012/7/15	5:05	3.9	0.5	0.0	0.0	0.0	
2012/7/20	22:10	10.7	24.0	22.7	21.3	20.8	
2012/7/21	20:25	0.6	0.5	0.0	0.0	0.0	
2012/7/22	15:45	0.3	0.5	0.0	0.0	0.0	
2012/8/5	23:50	0.9	0.5	0.0	0.0	0.0	
2012/8/12	3:00	1.1	8.5	8.0	7.7	6.9	
2012/8/13	13:25	0.3	3.5	2.3	0.3	2.0	
2012/8/13	20:20	11.3	31.0	28.3	27.3	26.1	Rain Event 2
2012/8/15	19:10	7.0	0.5	0.0	0.0	0.0	
2012/8/17	22:00	1.3	1.0	0.3	0.3	0.0	
Total for before-thinning period			204.2	182.3	175.9	170.9	
Thinned on August 23							
2012/8/24	17:35	2.0	0.5	0.0	0.3	0.2	
2012/8/27	17:10	0.9	3.0	2.0	1.0	1.5	
2012/8/30	7:30	0.8	0.6	0.3	0.3	0.3	
2012/8/30	20:00	5.3	0.5	0.0	0.3	0.3	
2012/9/1	16:25	1.8	5.5	4.3	3.7	3.9	
2012/9/4	12:05	2.7	6.8	5.7	5.3	5.6	
2012/9/6	8:20	3.5	27.0	24.7	22.0	23.7	
2012/9/11	9:35	13.8	18.2	16.3	14.3	15.3	
2012/9/12	16:40	0.7	5.3	4.7	4.3	4.8	
2012/9/15	22:50	3.3	1.5	1.0	1.0	0.6	
2012/9/23	4:05	13.7	14.8	13.0	12.3	13.0	
2012/9/24	1:10	18.2	36.4	32.0	30.0	31.9	Rain Event 3
2012/9/25	9:05	0.1	0.5	0.0	0.0	0.0	
2012/9/30	17:10	23.1	84.9	77.3	67.6	79.0	Rain Event 4
2012/10/2	0:55	5.7	2.0	1.7	1.7	1.7	
2012/10/2	22:50	3.3	1.4	0.7	1.0	0.8	
2012/10/5	2:55	0.4	2.0	1.7	1.7	1.4	
2012/10/6	20:15	6.8	4.5	3.7	3.3	3.4	
2012/10/11	17:35	10.4	10.8	9.3	8.7	9.1	
2012/10/13	6:00	2.2	1.5	1.0	1.3	0.9	
2012/10/15	11:05	0.8	2.0	1.3	1.3	1.4	
2012/10/17	15:00	26.9	33.0	29.3	26.7	29.0	
2012/10/23	7:30	26.3	28.0	24.3	19.7	24.1	
2012/10/25	21:45	6.8	0.7	0.3	0.3	0.2	
Total for after-thinning period			291.5	254.6	228.2	251.8	

Table 3 Amount of rainfall and canopy interception before and after thinning for each tray.

	P_G	Number of rain events	Tray number	I	I'	I / I'	I/P_G	I_R	I_{R_PM}	I_{SDE}	I_{Sbt}	I_{Sbt_PM}	I_{Aft}	I_R/ I	I_{SDE}/ I
	(mm)			(mm)	(mm)	(%)	(%)	(mm)	(mm)	(mm)	(mm)	(mm)	(mm)	(%)	(%)
Before thinning	204.2	16	1	22.0	23.5	93.6	10.8	14.8	3.4	11.4	-0.8	17.0	9.5	67.3	52.0
			2	28.3	29.8	95.0	13.9	21.2	4.7	16.5	-1.5	21.7	10.1	74.9	58.3
			3*	33.4	36.1	92.5	16.3	24.3	4.9	19.4	-2.1	22.6	13.9	72.8	58.0
After thinning	291.5	24	1	37.0	36.3	101.9	12.7	26.1	16.5	9.6	-1.7	11.1	11.9	70.5	26.0
			2	63.3	63.2	100.2	21.7	59.4	20.9	38.5	-2.0	14.3	5.8	93.8	60.9
			3	39.7	38.1	104.2	13.6	28.7	22.4	6.3	-0.9	15.0	10.3	72.3	15.9

* In the rain event on July 6 (Rain Event 1) in Table 2 I_R and I_{Sbt} were not obtained independently due to clogging up of the drain, but the total value of I_R + I_{Sbt} was measured. In the event it was assumed that I_{Sbt} = 0 based on the results as shown in Figure 2 and that $I_R + I_{Sbt} = I_R$.

Table 4 Amount of rainfall and canopy interception during four heavy rain events.
Each value represents the total amount, although the sum operator is omitted.

	Rain Event	P_G	Number of sub-rain events	Tray number	I	I'	I / I'	I/P_G	I_R	I_{R_PM}	I_{SDE}	I_{Sbt}	I_{Aft}	I_R/ I	I_{SDE} / I
		(mm)			(mm)	(mm)	(%)	(%)	(mm)	(mm)	(mm)	(mm)	(mm)	(%)	(%)
Before thinning	1	110.2	22	1	8.9	9.5	94.4	8.1	8.8	1.6	7.2	-0.5	1.1	98.3	80.5
				2	8.6	9.5	90.9	7.8	9.2	2.2	7.0	-1.2	1.5	106.8	81.2
				3 *	11.7	14.5	81.0	9.6	–	2.3	–	–	2.2	–	–
	2	31.0	6	1	2.7	2.6	102.6	8.6	2.5	-0.2	2.7	-0.6	0.7	93.4	100.8
				2	3.7	3.6	101.9	11.9	3.5	-0.2	3.7	-0.6	0.7	95.2	100.6
				3	4.9	5.0	99.2	15.9	3.4	-0.2	3.6	-0.3	1.8	69.1	73.1
After thinning	3	36.4	14	1	4.4	4.1	108.1	12.2	5.4	2.9	2.5	-1.2	-0.1	121.7	56.4
				2	6.4	6.4	100.0	17.7	6.9	3.2	3.7	-0.2	-0.2	107.2	57.5
				3	4.5	4.5	100.5	12.4	4.6	4.0	0.6	-0.4	0.2	102.1	13.3
	4	84.9	8	1	7.6	7.6	100.0	9.0	7.0	1.7	5.3	0.1	0.5	91.9	69.5
				2	17.3	17.3	100.0	20.4	16.3	2.2	14.1	0.4	0.6	94.3	81.6
				3	6.0	5.8	103.6	7.0	4.4	2.4	2.0	0.3	1.0	73.7	33.5

* I_R and I_{Sbt} were not obtained due to clogging up of the drain, and I_{SDE} was not calculated.

Appendix B

Table B1 List of acronyms, abbreviations and symbols.

Symbol	Unit	Description
γ	K^{-1}	Psychrometric constant
Δ	K^{-1}	Slope of the saturated specific humidity versus temperature curve
ΔS	mm	Difference in water storage between t_{Ren} and t_{Rel}
ΔS_{Bi}	mm	Difference in water storage between t_{Bei} and t_{Bsi}
ΔS_{Ri}	mm	Difference in water storage between t_{Rei} and t_{Rsi}
Δt	h	Time interval (5 minutes)
λ	J kg^{-1}	Latent heat of vaporization
ρ	kg m^{-3}	Air density
C_P	J kg^{-1} K^{-1}	Specific heat of air
D	mm h^{-1}	Drainage rate from the tray
d	m	Zero plane distance
E	mm h^{-1}	Evaporation rate during rain event
E_{cal}	mm h^{-1}	Calculated evaporation rate
E_{PM}	mm h^{-1}	Calculated evaporation rate using the Penman–Monteith equation
G	W m^{-2}	Ground heat flux
I	mm	Canopy interception
i	–	Ordinal number for the sub-rain event or the storm break time: i = 1, 2, • • • , n
I'	mm	Canopy interception calculated as the sum of I_R, I_{Sbt} and I_{Aft}
I_{Aft}	mm	Canopy interception after cessation of rainfall
I_{jAft}	mm	Canopy interception after cessation of rainfall for Tray j
I_{jR}	mm	Canopy interception during rainfall for Tray j
I_{jRi}	mm	Canopy interception during rainfall for Tray j for the i-th sub rain event
I_{jR_PMi}	mm	Canopy interception during rainfall for Tray j for the i-th sub rain event calculated using the Penman–Monteith equation
I_{jSbt}	mm	Canopy interception during storm break time for Tray j
I_{jSbti}	mm	Canopy interception during storm break time for Tray j for the i-th storm break time

I_{jSbt_PMi}	mm	Canopy interception during storm break time for Tray *j* for the *i*-th storm break time calculated using the Penman–Monteith equation
I_R	mm	Canopy interception during rainfall
I_{Ri}	mm	Canopy interception during rainfall for the *i*-th sub rain event
I_{R_PM}	mm	Canopy interception during rainfall calculated using the Penman–Monteith equation
I_{R_PMi}	mm	Canopy interception during rainfall for the *i*-th sub rain event calculated using the Penman–Monteith equation
I_{Sbt}	mm	Canopy interception during storm break time
I_{Sbti}	mm	Canopy interception during storm break time for the *i*-th sub rain event
I_{Sbt_PM}	mm	Canopy interception during storm break time calculated using the Penman–Monteith equation
I_{Sbt_PMi}	mm	Canopy interception during storm break time for the *i*-th storm break time calculated using the Penman–Monteith equation
I_{SDE}	mm	Canopy interception during rainfall caused by splash droplet evaporation
j	–	Ordinal number for the tray: j = 1, 2 and 3
k	–	von Karman constant
n	–	Number of sur-rain events
P_G	mm	Gross rainfall
P_{Gi}	mm	Gross rainfall for the *i*-th sub-rain event
PM	–	Penman–Monteith (equation)
P_N	mm	Net rainfall
PVC	–	Polyvinyl chrodride
q	kg kg^{-1}	Specific humidity
q_s	kg kg^{-1}	Saturated specific humidity
R	mm h^{-1}	Rainfall rate
r^2	–	Determination coefficient
r_a	s m^{-1}	Aerodynamic resistance
RH	%	Relative humidity
R_n	W m^{-2}	Net radiation
S	mm	Water storage
S_j	mm	Water storage for Tray *j*
Sbt	h	Storm break time
SDE	–	Splash droplet evaporation
Spt	h	Separation time to divide rainfall into two independent rain events

T_a	ºC	Air temperature
t_{Bei}	h	Time of the end of the *i*-th storm break
t_{Bsi}	h	Time of the start of the *i*-th storm break
t_{Rei}	h	Time of the end of the *i*-th sub-rain event
t_{Rsi}	h	Time of the start of the *i*-th sub-rain event
u	m s^{-1}	Wind speed
z	m	Reference height
z_0	m	Roughness height length

Figure captions

Figure 1. Arrangement of Trays 1, 2 and 3 before thinning. Note that Tray 1 and Tray 2 were inclined so rainwater drained. In Trays 1 and 2, the height difference between the front right corner and far left corner where the drains were made was ~10 cm.

Figure 2. Relationship between gross rainfall P_G and observed canopy interception during rainfall I_R, during storm break time I_{Sbt}, and after cessation of rainfall I_{Aft}, on a rain event basis. (a) Tray 1 (control), (b) Tray 2 before thinning, (c) Tray 3 before thinning; (d) Tray 1 (control); (e) Tray 2 after thinning, (f) Tray 3 after thinning. In the panel (c) for the largest P_G of 110.2 mm, the sum of I_{3R} and I_{3Sbt} is shown due to the clogged drain.

Figure 3. Observed and calculated canopy interception during rainfall (respectively, I_R and I_{R_PM}) and during storm break time (respectively, I_{Sbt} and I_{Sbt_PM}), against gross rainfall P_G. (a) Tray 1 (control), (b) Tray 2 before thinning, (c) Tray 3 before thinning; (d) Tray 1 (control), (e) Tray 2 after thinning, (f) Tray 3 after thinning. Observed values and regression lines are the same as those in Fig. 2.

Figure 4. (a)–(d): Gross rainfall for the *i*-th sub-rain event P_{Gi} and observed canopy interception during rainfall for the sub-rain event I_{jRi} in Tray *j* for four heavy rain events. (e)–(h): Calculated canopy interception during rainfall for *i*-th sub-rain event I_{jR_PMi} and that of observed I_{jRi} for four heavy rain events in Tray *j*. (a) and (e): Rain Event 1 with total gross rainfall (P_G) of 110.2 mm before thinning period; (b) and (f): Rain Event 2 with P_G of 31.0 mm before thinning period; (c) and (g): Rain Event 3 with P_G of 36.4 mm after thinning period; (d) and (h): Rain Event 4 with P_G of 84.9 mm after thinning period.

Figure 5. Observed canopy interception during storm break time I_{jSbti} and calculated I_{jSbt_PMi} on a storm break time basis in Tray *j*. (a) Rain Event 1 before thinning period; (b) Rain Event 2 before thinning period; (c) Rain Event 3 after thinning period; (d) Rain Event 4 after thinning period.

Figure 6. Time series of water budget, canopy interception and meteorological elements for Rain Event 1 with total gross rainfall P_G of 110.2 mm, before thinning: (a) P_G; (b) canopy storage *S*; (c) observed cumulative I_{jRi}; (d) calculated cumulative I_{jR_PMi}; (e)

observed cumulative I_{jSbti}; (f) calculated cumulative I_{jSbt_PMi}; (g) calculated potential evaporation E_{PM}; (h) net radiation R_n; (i) relative humidity RH; (j) air temperature T_a; (k) wind speed u. Unit of ordinates is mm unless otherwise indicated.

Figure 7. Time series of water budget, evaporation and meteorological elements for Rain Event 4 with total gross rainfall P_G of 84.9 mm, after thinning; details on each panel are the same as in Fig. 6.

Figure 8. Dependence of lifetime for small droplets on relative humidity RH and air temperature. (a) RH=95%; (b) RH=99%.

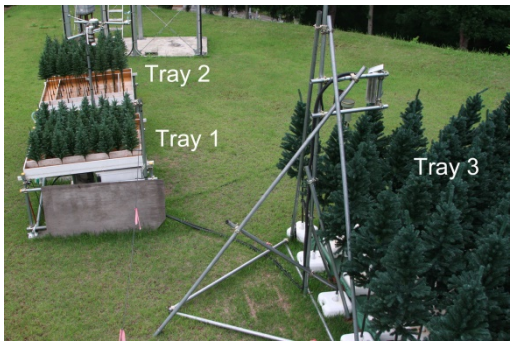

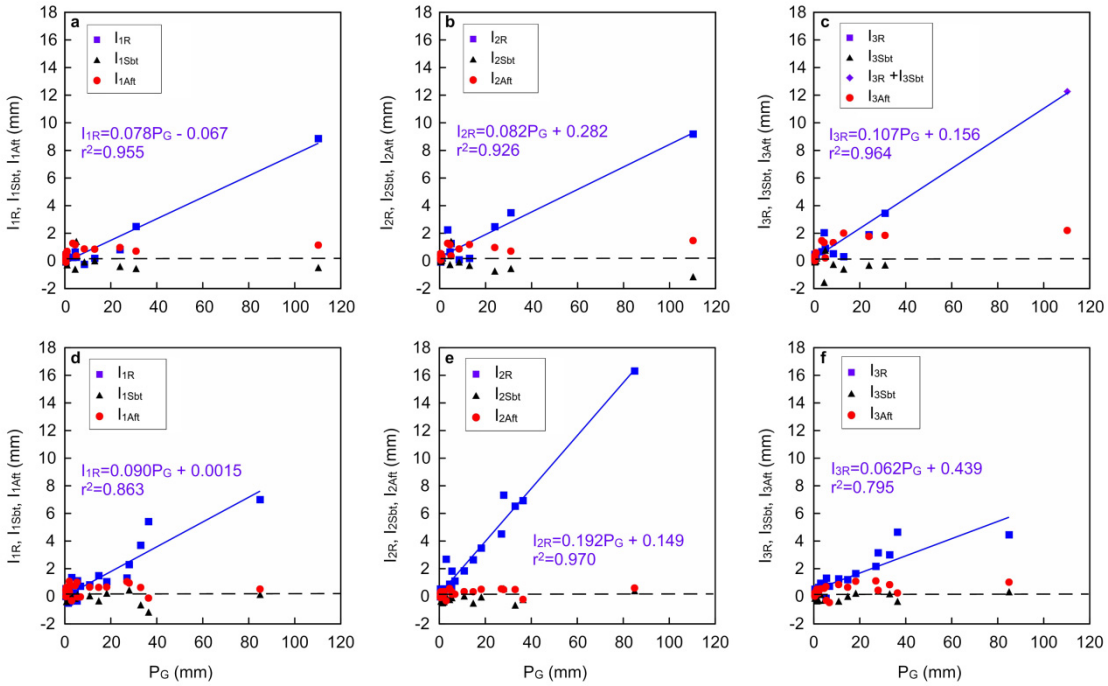

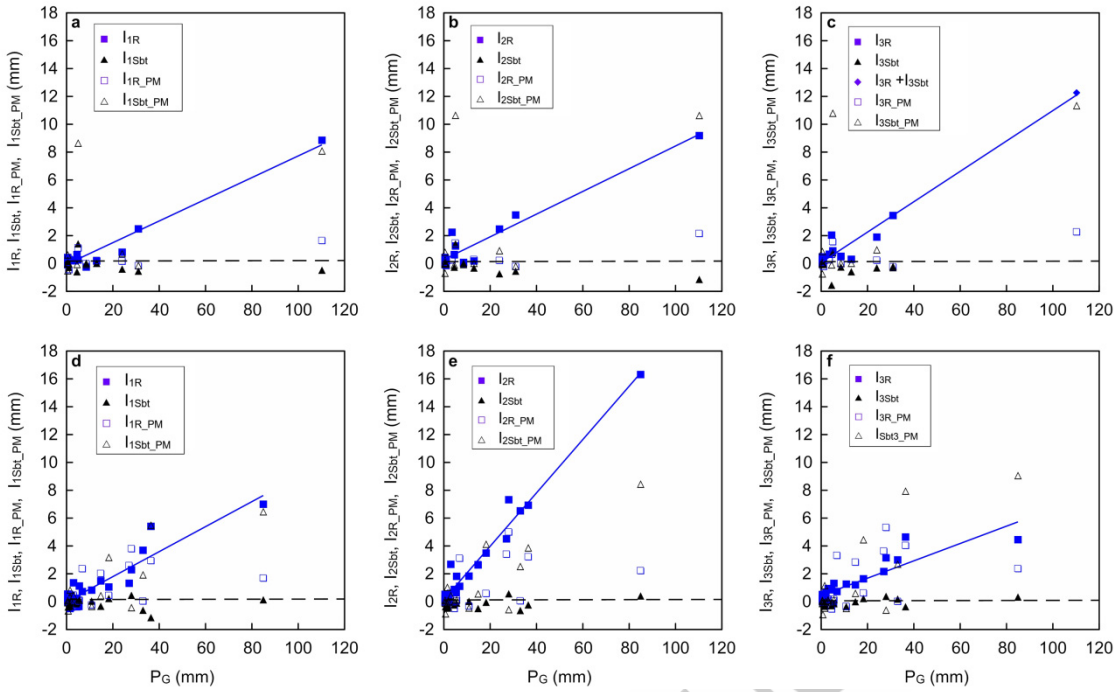

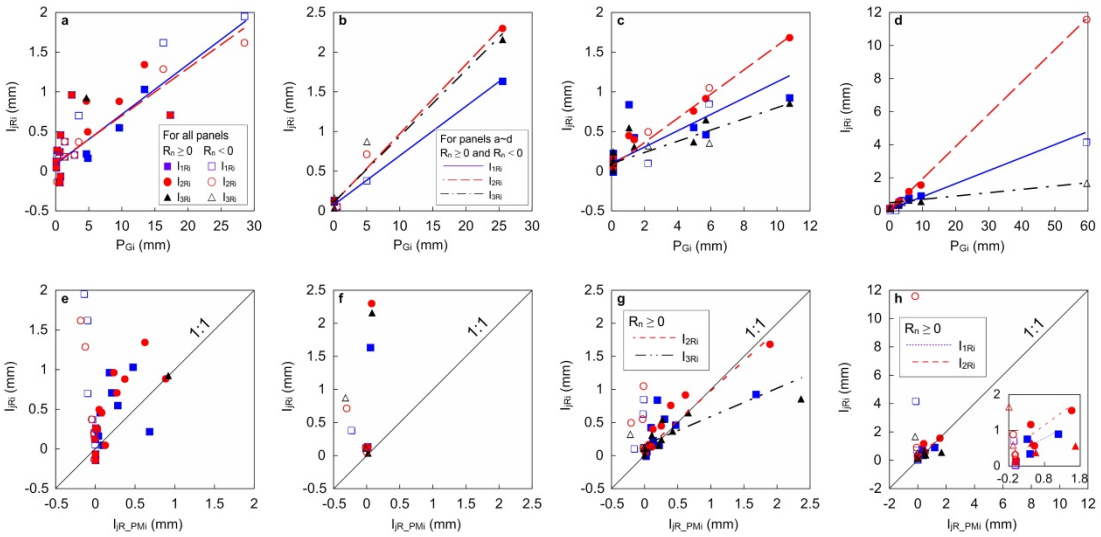

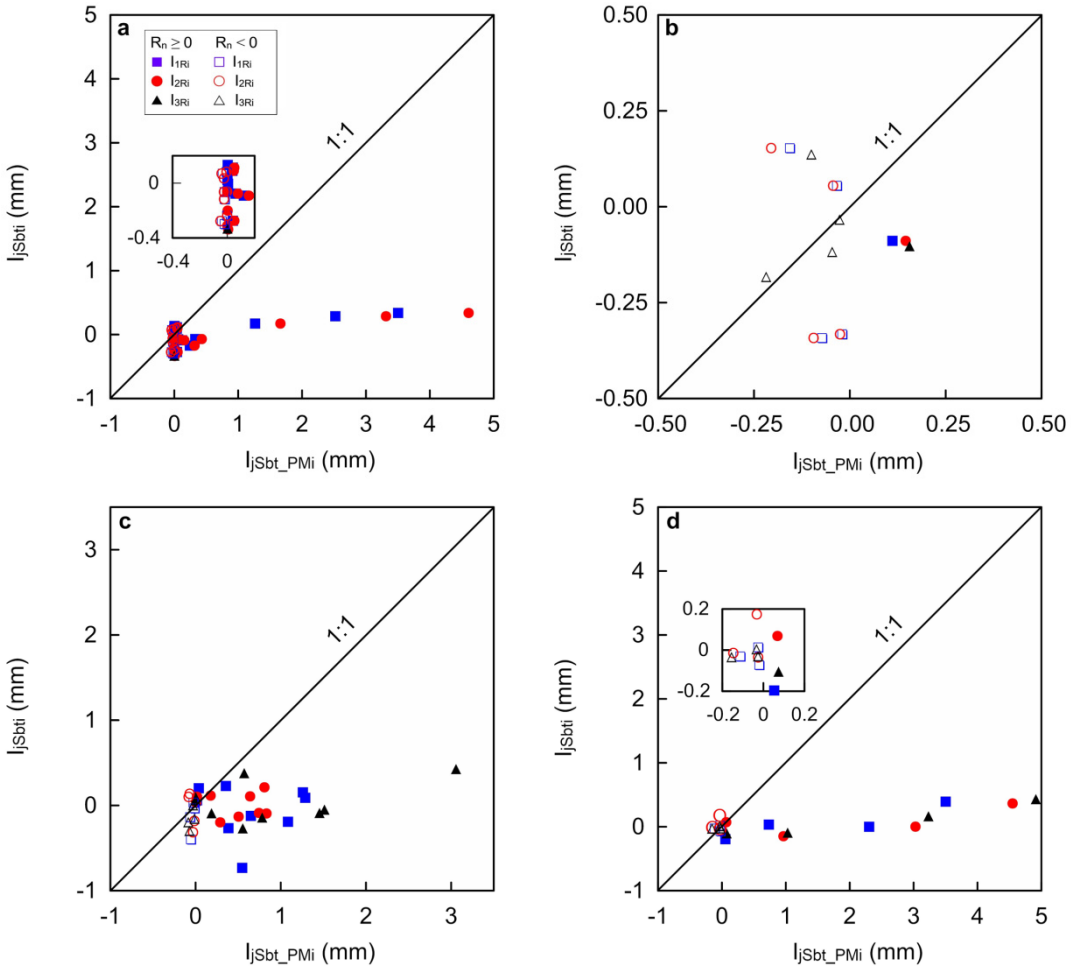

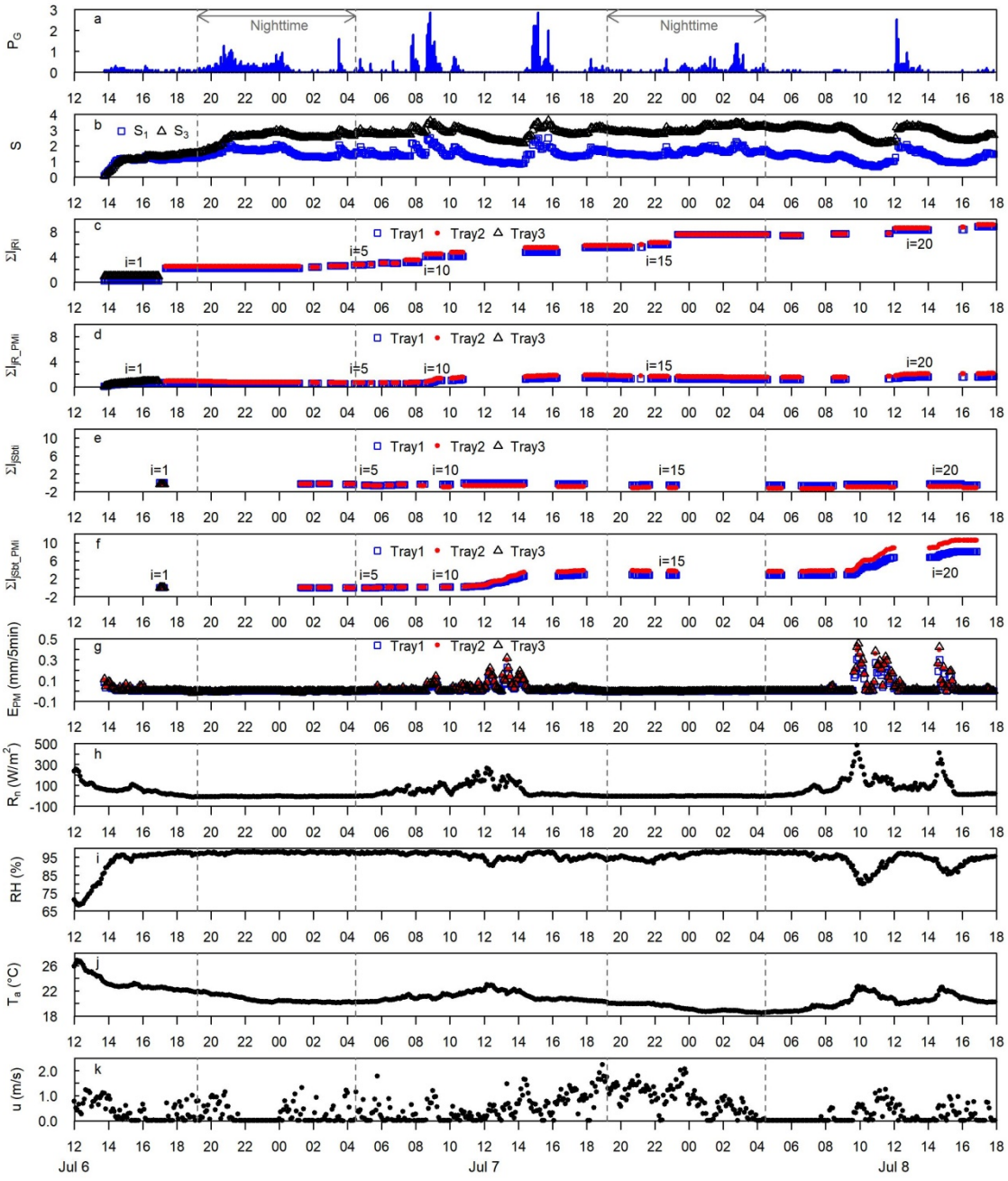
a
Nighttime
Nighttime
P_G
b
S_1 S_3
S
c
Tray1 Tray2 Tray3
i=1
i=5
i=10
i=15
i=20
ΣI_{IR}
d
Tray1 Tray2 Tray3
ΣI_{IR_PMI}
e
Tray1 Tray2 Tray3
ΣI_{Std}
f
Tray1 Tray2 Tray3
ΣI_{Std_PMI}
g
Tray1 Tray2 Tray3
E_{PM} (mm/5min)
h
R_n (W/m^2)
i
RH (%)
j
T_a (°C)
k
u (m/s)
Jul 6
Jul 7
Jul 8

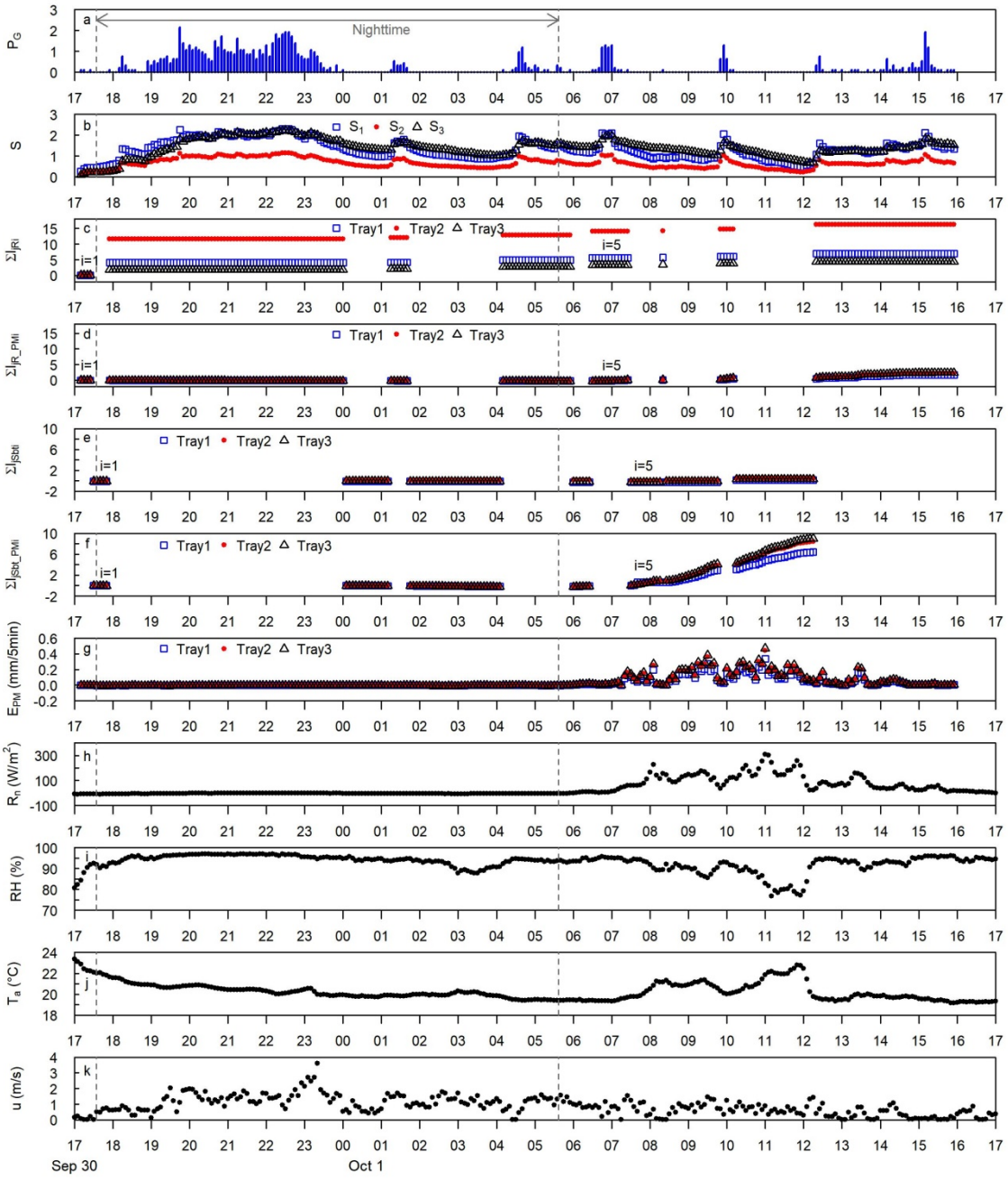
a
Nighttime
P_G
b
S_1 S_2 S_3
S
c
Tray1 Tray2 Tray3
i=1
i=5
ΣI_{IR}
d
Tray1 Tray2 Tray3
i=1
i=5
ΣI_{IR_PMI}
e
Tray1 Tray2 Tray3
i=1
i=5
ΣI_{Std}
f
Tray1 Tray2 Tray3
i=1
i=5
ΣI_{Std_PMI}
g
Tray1 Tray2 Tray3
E_{PM} (mm/5min)
h
R_n (W/m^2)
i
RH (%)
j
T_a (°C)
k
u (m/s)
Sep 30
Oct 1